A porous-crust drying model for a single dairy droplet

O'Connell, Ken; Olaleye, Akeem K.; Van den Akker, Harry E.A.

DOI
10.1016/j.cherd.2023.11.040

Publication date
2023

Document Version
Final published version

Published in
Chemical Engineering Research and Design

Chemical Engineering Research and Design 200 (2023) 741–752

Contents lists available at ScienceDirect

Chemical Engineering Research and Design

journal homepage: www.elsevier.com/locate/cherd

A porous-crust drying model for a single dairy droplet

Ken O'Connell [a], Akeem K. Olaleye [a], Harry E.A. Van den Akker [a,b,c,*]

[a] Dairy Processing and Technology Centre, University of Limerick, Limerick, Ireland
[b] Bernal Institute, University of Limerick, Limerick, Ireland
[c] Section Transport Phenomena, Department of Chemical Engineering, Delft University of Technology, Delft, Netherlands

ARTICLE INFO

Keywords:
Dairy powder
Drying kinetics
Single droplet drying
Porous crust
Numerical modelling

ABSTRACT

The development of a novel numerical model for droplet drying is the topic of this paper. The three main stages of droplet drying are distinguished, viz. unhindered evaporation of a 'wet' particle (the droplet), restricted drying at a falling rate due to the formation of a crust around a wet core, and inert heating of the dry porous particle. Each stage is mathematically detailed to replicate all phenomena occurring throughout the drying process. The focus, however, is on the falling rate drying regime which is described in terms of Stefan diffusion of water vapour through the pores of a thickening crust. To this end, the model needs the material properties. This permits the droplet characteristics to be determined by composition rather than through single-droplet drying experiments. Finally, the model is validated against five of such experiments from literature using skim milk. Good agreement is found at each comparative case for the particle mass and temperature throughout the various drying regimes providing that for good reasons in three cases a lower drying air temperature is applied than reported for the experiments. The model is capable of predicting the entire drying process at low computational cost and without requiring empirical input.

1. Introduction

1.1. Background

Spray drying is an old process widely used in the pharmaceutical and food industry for converting a liquid into a powder (Cal and Sollohub, 2010; Sollohub and Cal, 2010; Sharma et al., 2012; Shishir and Chen, 2017). To this end, a liquid feed stock is forced through an atomization device and sprayed from above into a large and wide tower or chamber, while high-temperature air is fed into the tower or chamber, either from the top or from the bottom part, to provide the heat required for evaporating the liquid solvent, usually water. As the droplets fall to the base of the tower or chamber, they change from liquid droplets first into wet particles and finally into a dried powdered product.

Although the principle of spray drying looks simple, it actually is a complex interplay of atomization, drying air hydrodynamics, particle motions, heat and mass transfer, and evaporation, where variations in feed stock properties, operating conditions, and droplets varying in size are complicating factors. In this paper, we will model and simulate the entire drying process of a single dairy (skim milk) droplet all the way to a dry porous particle with the view of contributing to improving spray drying operations in the dairy industry.

Most operators of dairy plants rely on hands-on expertise gathered over time as to how to operate their spray dryer for slightly varying conditions. Usually, they hesitate to improve or optimize their spray drying process stepwise, e.g. by installing an ultrasonic atomizer, as this implies entering unexplored territory. In addition, embarking on an experimental test program in the plant to explore improvement options is very costly and considered risky — factors impeding innovation.

Computational modelling, more specifically Computational Fluid Dynamics (CFD), may serve as an alternative approach allowing the evaluation and assessment of a whole range of design variables and operating conditions before the best one or the two most promising options will be tested in the commercial plant, thereby reducing costs and risks. Many studies have been reported (Kieviet and Kerkhof, 1997; Harvie et al., 2001; Saleh, 2010; Gabites et al., 2010; Woo et al., 2012; Mezhericher et al., 2015; Saleh and Hameed, 2016) on the air flow patterns within spray dryers. The main challenge now is about how to incorporate the key drying process into the CFD software for the flow patterns of the drying air.

* Corresponding author at: Bernal Institute, University of Limerick, Limerick, Ireland.
E-mail address: harry.vandenakker@ul.ie (H.E.A. Van den Akker).

https://doi.org/10.1016/j.cherd.2023.11.040
Received 22 April 2023; Received in revised form 12 October 2023; Accepted 20 November 2023
Available online 22 November 2023

While it is rather straightforward to simulate the external heat and mass transfer to and from the droplets, the drying kinetics of the particles is much more complex and should include the internal resistances to heat and mass transfer which increase as the liquid evaporates and a thickening crust around a wet core is formed. Various approaches are reported in the literature, see e.g. the reviews by Cal and Sollohub (2010), by Mezhericher (Mezhericher et al., 2010a, 2011, 2012) and by Shishir and Chen (2017), varying from simply using experimental information on the overall drying rate of a droplet all the way to explicitly solving the heat and mass transport equations within a droplet during the drying process.

A handicap for validating computational models for dairy materials is that very few experimental data are available in the literature, because drying experiments are tedious and expensive (Mezhericher et al., 2010b). A limited number of papers is reporting about drying experiments on single skim milk droplets suspended in a hot, usually vertical, air flow. Early experiments of this type were carried out at the University of Wisconsin by Charlesworth and Marshall (1960) and by Trommelen and Crosby (1970). Further experiments in essentially the same type of test rig were reported by Sano and Keey (1982) and by Nešić (Nešić, 1989; Nešić and Vodnik, 1991). Many more papers on drying dairy droplets/particles were published by researchers at the University of Auckland, New Zealand (Stevenson et al., 1998; Chen et al., 1999; Lin and Chen, 2002; Farid, 2003). In our validation study, experimental data reported by Lin and Chen (2002), by Chen et al. (1999) and by Nešić (Nešić, 1989; Nešić and Vodnik, 1991) were used.

1.2. About modelling

The simplest droplet drying approach makes use of the concept of a characteristic drying curve (CDC) which is based on the hypothesis – see Langrish and Kockel (2001) – that the drying process for a given material can largely be described by a linear falling rate curve which is independent of gas temperature, humidity and velocity. This drying rate only depends on the averaged moisture content of the droplet (Saleh, 2010). The CDC approach exploits experimental data obtained by measuring the drying rate of a single, rather large (1.5–2.0 mm) droplet of the material of interest when suspended in an air flow, as reported by some authors (Nešić, 1989; Chen et al., 1999; Lin and Chen, 2002). The resulting CDC can be incorporated into any CFD code. This combined CFD-CDC method is attractive in terms of calculation time and is therefore used widely, e.g. by Saleh (2010) and Jaskulski et al. (2018). Its universal applicability, however, is dubious due the strongly simplified model and the use of empirical data which may not fit the large variety in dairy products and drying conditions.

An alternative method for predicting the drying behaviour of particles is the so-called reaction engineering approach (REA) which aims at describing profiles of moisture and temperature versus time. In addition to mass and heat balances along with heat and mass transfer coefficients, the concept of an activation energy is applied that relates the partial vapour density at the droplet surface to the saturated vapour concentration, see e.g. Chen (2008) and Haque et al. (2016). The REA approach can be applied in both a lumped and a spatially resolved mode, see e.g. Chen and Putranto (2015) and Putranto and Chen (2015), and it can be implemented as an individual Matlab code, see e.g. Chen and Putranto (2015), or into CFD software, see e.g. Jin and Chen (2009).

A completely deterministic approach looks at solving the various energy, mass and species equations explicitly, not only for the gas phase but also for the interior of the drying particles. The spatial distributions of temperature, water concentration and solids content within the droplet are resolved as a function of time (Mezhericher et al., 2015). Such computational simulations should describe how fast the moisture is transported from the interior of a particle towards its surface where the evaporation takes place. After some initial phase, one could think in terms of a wet core surrounded by a (dry) crust, with an interface receding towards the centre of the particle. The complexity of a moving boundary with mass transport and thermal effects creates a significant computational task (Mezhericher et al., 2010a). While the use of such deterministic models may provide detailed insight in the drying dynamics of single droplets, their inherent computational demands prohibit incorporating them into spray drying simulations of industrial spray driers.

In this paper, we present a somewhat simplified approach for describing the drying kinetics of a dairy particle. Just like in Mezhericher's model, also used by Mortier et al. (2012) for single pharmaceutical granules, and in the model proposed by Sadafi et al. (2014, 2015), the droplet develops a porous crust surrounding a wet core and increasing in thickness over time. Moroney and Vynnycky (2021) also used a model involving a receding porous crust (or a shrinking core) for describing the release of an active pharmaceutical ingredient (API) from a porous granule. The concept finds support in images obtained by time-resolved X-ray micro-tomography with UV/visible spectrophotometry of acetaminophen dissolution from granules (Kašpar et al., 2013).

In our approach, we ignore spatial variations in temperature inside the drying particle. This looks as being permitted, not only thanks to own exploratory simulations but also as Mezhericher et al. (2007) in their simulations of drying a skim milk particle found a minor temperature difference only between wet core and crust. This simplification substantially reduces the demanding numerical scheme of the Mezhericher approach. The method proposed also avoids the expensive experimentation needed in the CDC and REA methods outlined above. The novel model for (spray) drying dairy products has been validated with the help of experimental data from the literature on the drying of a single droplet containing skim milk powder (SMP). This novel approach will allow for the implementation of the pertinent code into (commercial) CFD software for simulating the behaviour and performance of industrial-scale spray dryers.

2. Model development

This section describes the various stages of drying from droplet to a dry particle. We consider a single (stationary) SMP particle positioned in a uniform air flow field, while for the time being we ignore the effect of air humidity. In all stages of the drying process, the vapour – whether formed at the particle surface or arriving from the interior – is advected away by the air flow field, while the heat for the evaporation is supplied from the air flow field. The mathematical model in each of these stages is different — reason why we have to distinguish between the various stages.

2.1. Droplet drying stages

Producing a solid dairy particle from a droplet by evaporating the water goes through different stages, as shown in Fig. 1 that shows the temperature profile of a droplet as a function of time. At point 0 in the figure, the droplet is exposed to hot air and a, usually short, heating stage sets in. As a result, the evaporation rate increases, consuming heat to an increasing extent. Eventually, at point 1, the heat consumption due to evaporation matches the external heat supply. The pertinent temperature is denoted as the wet bulb temperature, always lower than the ambient gas phase temperature, satisfying this matching condition.

In this regime, which lasts as long as the surface of the particle remains wet (owing to supply of water from inside), the drying rate and the (surface) temperature remain constant, determined by the equilibrium between heat consumption through evaporation and supply of heat from the ambient air. In this stage, the droplet shrinks.

The presence of the dairy components in the droplet may reduce the evaporation rate as part of the droplet's surface is occupied by solute. In the current model, this so-called solute effect – see e.g., Rezaei and Netz (2021) – is ignored in the pre-crust stage.

The temperature of the droplet (surface) remains constant until a crust starts being formed at point 2, as the rate of moisture transport from the interior can no longer keep up with the rate of evaporation from the surface. As the evaporation continues, the crust becomes thicker and thicker as a result of which the resistance to evaporation keeps increasing and the drying rate falls, while now the core is shrinking.

In this stage of the drying process, the droplet transforms into a particle (with a solid crust and a wet core). From now on, in describing the drying process, we will often just speak about a 'particle' irrespective of how much of it is in the liquid phase.

At the end of the drying process, after a final (bounded) moisture content has been attained at point 3, or after in our simulation the evaporation rate in a time step has turned larger than the amount of liquid present in the core, inert heating takes place.

In all stages of the drying process, a uniform temperature distribution within the particle is assumed on the basis of an analysis in terms of the Biot number, Bi, which is given by

$$\mathrm{Bi} = \frac{hL_c}{k} \tag{1}$$

where h is the external convective heat coefficient between droplet and gas flow, L_c is the characteristic length of the sphere (volume over surface area) and k is the thermal conductivity of the droplet. This Bi stands for the ratio of the external convective heat transport towards the particle and the internal conductive heat transport. Typical spray conditions and small droplet diameters (say, smaller than 1 mm) result in Bi ≤ 0.1, as observed by several authors (Mezhericher et al., 2008; Gopireddy and Gutheil, 2013). Then, temperature may be taken uniform within the droplet allowing for a lumped analysis (Deen, 1998). [Note this is different from the case of a dissolving API (Moroney and Vynnycky, 2021) where the dissolution takes place in a liquid and Bi > 1.] When validating the model, this uniform particle temperature is compared with the (average) particle temperature measured in drying experiments on single drops in the 1 to 2 mm range.

While the stages of constant drying rate and inert heating can readily be described by standard heat transport theory, the focus of our paper is on the modelling and simulation of the falling drying rate regime. Key in this regime is the increasing resistance to vapour and heat transport due to the growing crust surrounding the liquid core. The novelty of our paper is in the way we deal with this time-dependent crust resistance, along with the Biot number supported assertion that the temperature within the particle may be taken as uniform. Before presenting all equations used in the code simulating the entire drying process, first the basis of our novel approach of the falling rate regime will be explained in conceptual terms, without equations.

2.2. Model assumptions for the falling drying rate

Our model is a new attempt to describe the vapour and heat transport through a porous crust growing in thickness. We tried to conceive how, in the falling rate regime, the heat penetrates through the crust, how and where the liquid evaporates due to the arrival of heat, and how the vapour escapes. The eventual set of conceptual propositions that has resulted in useful and successful simulations (reported further on) is as follows:

- The 'particle' is spherical, remains spherical while drying (no implosions or outbursts), and keeps its integrity (remains intact). Particle shrinkage as described by e.g. Jubaer et al. (2018) is ignored.
- The only mass transport inside the particle considered is that of water vapour; the dairy components locally precipitate when and where the water evaporates, and they stay wherever they precipitate. This implies that the eventual particle is porous, the spatial structure and composition being uniform and remaining steady.

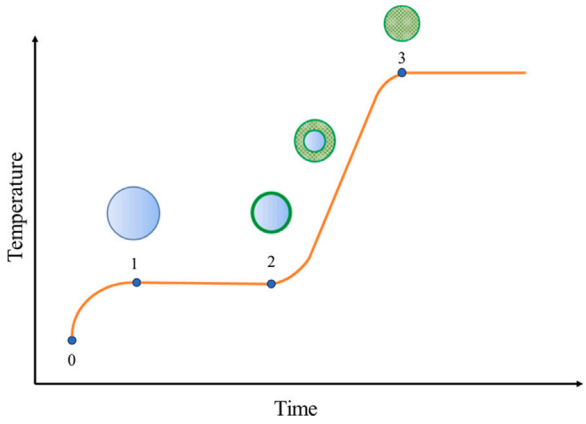

Fig. 1. The various drying stages for a droplet from its introduction into hot air all the way to the eventual porous solid particle still containing bounded moisture. Shrinkage of the particle only takes place in the range 1 to 2 when the evaporation takes place from the surface.
Source: Figure adapted from Farid (2003) and Mezhericher et al. (2011, 2015).

- As the particle starts evaporating at the surface and the evaporation proceeds faster than the transport of moisture from the interior to the surface, at a specific moment in time, in a single time step of the simulation, a very thin crust is formed covering the entire surface that grows uniformly over time.
- As soon as a crust has been formed, the evaporation takes place at the boundary between wet core and porous crust, resulting in a shrinking wet core (Mezhericher et al., 2007; Mortier et al., 2012; Golman and Julklang, 2013) while the porous crust increases in thickness.
- The crust layer is of uniform porosity ε with pores homogeneously distributed across the crust (and eventually the particle), a substantial proportion of them being oriented such that they allow for unilateral diffusive vapour transport (according to Stefan's law, see e.g. Van den Akker and Mudde (2023)) through the crust towards the particle surface.
- The effect of the tortuosity of the pores on the rate of diffusion is taken into account by adding a factor ε^{β}, with empirical exponent β=1.9, to the expression for the Stefan diffusion flux, as done before (Archie, 1942; Mortier et al., 2012; Golman and Julklang, 2013).
- The vapour arrives from the interior via the pores in the crust at the particle surface and leaves from the pore mouths which occupy part ε of the particle surface.
- The transport of heat required for the evaporation at the boundary between wet core and crust takes place through conduction via the solid material of the crust only, which occupies part $(1-\varepsilon)$ of the particle surface, since the outward bounded diffusive vapour transport through the pores may efficiently impede conduction of heat in the vapour phase in the opposite direction.
- In the simulations, we did not include the so-called Spalding (blowing) coefficients (Zhifu et al., 2013; Sadafi et al., 2014; Sazhin, 2017; Strizhak et al., 2018), which are quite common in modelling fuel droplet evaporation at high temperatures with the view of considering Stefan mass and heat transport. Under the conditions pertinent to a spray dryer with water as the evaporating liquid, these coefficients are negligibly small.

2.3. The equations for the constant drying rate regime

The initial evaporation of a droplet after abrupt exposure to a steady and uniform hot air flow can be described as unhindered drying. Due to the high liquid content of the droplet and given the uniform droplet temperature assumption (because of Bi $\leq$ 0.1), the following single

equation can be used to describe the heat transfer to the droplet both in the initial heating period and in the subsequent wet bulb temperature regime:

$$\frac{dT_p}{dt} = h\left(T_g - T_p\right)\frac{4\pi R_p^2}{c_{p,p}m_p} - \frac{h_{fg}\dot{m}}{c_{p,p}m_p} \tag{2}$$

where T_p is the droplet temperature, T_g is the gas (air) temperature, R_p is the particle radius, $c_{p,p}$ is the specific heat of the particle and m_p is the particle mass. The negative term accounts for the evaporation impact, where h_{fg} is the latent heat of evaporation and $\dot{m}$ is the mass flow rate of liquid from the particle.

The external heat transfer coefficient, h, is dependent on the Nusselt number, Nu, obeying the well-known correlation due to Ranz and Marshall (1952):

$$\mathrm{Nu} = \frac{h2R_p}{k_g} = 2 + 0.6\mathrm{Re}^{1/2}\mathrm{Pr}^{1/3} \tag{3}$$

where k_g is the thermal conductivity of the gas phase. The particle Reynolds number, Re, and the Prandtl number, Pr, are given by:

$$\mathrm{Re} = \frac{\rho_g U_g 2R_p}{\mu_g} \tag{4}$$

$$\mathrm{Pr} = \frac{c_{p,g}\mu_g}{k_g} \tag{5}$$

respectively, where U_g is the relative gas velocity, ρ_g is the gas density, μ_g is the gas viscosity and $c_{p,g}$ the specific heat capacity of the gas. On the basis of own experiments, Lin and Chen (2002) arrived at a slightly modified correlation for Nu:

$$\mathrm{Nu} = \frac{h2R_p}{k_g} = 2.04 + 0.62\mathrm{Re}^{1/2}\mathrm{Pr}^{1/3} \tag{6}$$

The driving force for the evaporation is the difference between the saturation water vapour density at the surface of the droplet and the water vapour density in the bulk of the gas phase, ρ_v and ρ_∞, respectively, resulting in the following expression for the evaporation rate $\dot{m}$:

$$\dot{m} = h_D\left(\rho_v - \rho_\infty\right)4\pi R_p^2 \tag{7}$$

The external mass transfer coefficient, h_D, is calculated through the Sherwood number obeying the correlation due to Ranz and Marshall (1952):

$$\mathrm{Sh} = \frac{h_D 2R_p}{D_v} = 2 + 0.6\mathrm{Re}^{1/2}\mathrm{Sc}^{1/3} \tag{8}$$

where D_v is the diffusion coefficient of water molecules in the gas phase and Sc is the Schmidt number given by:

$$\mathrm{Sc} = \frac{\mu_g}{\rho_g D_v} \tag{9}$$

Lin and Chen (2002) acquired a slightly modified correlation for Sh:

$$\mathrm{Sh} = \frac{h_D 2R_p}{D_v} = 1.63 + 0.54\mathrm{Re}^{1/2}\mathrm{Sc}^{1/3} \tag{10}$$

In order to calculate ρ_∞ and ρ_v in Eq. (7), the ideal gas law is invoked. Hence, the following correlations to bulk vapour pressure, $P_\infty(T_g)$, and saturation vapour pressure, $P_v(T_p)$, can be used:

$$\rho_\infty = \frac{M_v P_\infty(T_g)}{\Re T_g} \tag{11}$$

$$\rho_v = \frac{M_v P_v(T_p)}{\Re T_p} \tag{12}$$

where M_v is the molar weight of water and $\Re$ is the universal gas constant.

As a result of the evaporation, the mass of the droplet decreases:

$$\frac{dm_d}{dt} = -\dot{m} \tag{13}$$

where the evaporation rate $\dot{m}$ is given by Eq. (7). Provided that only the liquid water evaporates, the new radius of the droplet after a time step Δt is calculated with the help of the above mass flow rate:

$$R_p^{n+1} = \sqrt[3]{\frac{4\pi/3(R_p^n)^3\rho_w - \dot{m}\Delta t}{4/3\pi\rho_w}} \tag{14}$$

where ρ_w is the water density. From the new values m_d^{n+1} and R_d^{n+1}, an updated density, ρ_d, is obtained:

$$\rho_d = \frac{m_d}{4/3\pi(R_p^{n+1})^3} \tag{15}$$

This increase in density reflects the increase of volume fraction, ϕ, of the dissolved dairy material as a result of the water evaporation. This ϕ can be calculated from:

$$\phi = \frac{\rho_d - \rho_w}{\rho_{SMP} - \rho_w} \tag{16}$$

where ρ_{SMP} stands for the true density of the skim milk material.

The regime of unhindered evaporation lasts as long as the liquid volume fraction $(1-\phi)$ remains larger than a so-called critical moisture content. As soon as $(1-\phi)$ reaches this critical moisture content and more water evaporates, the dissolved solids (SMP) starts precipitating, to begin at the external surface of the droplet, forming a crust with porosity ε equal to $(1-\phi)$. Providing that the particle dries uniformly and no cavities are formed, this ε is equal to the porosity of the eventual dry powder particle:

$$\varepsilon = 1 - \frac{\rho_p}{\rho_{SMP}} \tag{17}$$

where ρ_p denotes the density of the crust and the eventual dry powder particle.

2.4. The equations for the falling drying rate regime

When the critical moisture content has been reached, a crust starts being formed. The evaporation now takes place at the interface of crust and wet core. This crust affects the drying process in three ways:

- The surface area available for heat transfer from the air has changed: the heat transfer from the air now only takes place to the solids fraction, 1-ε, of the crust, resulting in a reduced heat supply;
- The heat supply to the wet core is now restricted not only by the external heat transfer coefficient but also by the conductive heat transfer within the crust material; this is implemented by using an overall heat exchange coefficient U governing the heat transfer from outside to the wet core;
- At the crust–core interface, the heat supply is via the solids fraction, 1-ε, of the crust, while the vapour formed can only escape through the pores, being fraction ε of the crust; this effect is expressed by multiplying the evaporation rate by a factor α given by:

$$\alpha = \frac{1-\varepsilon}{\varepsilon} \tag{18}$$

We therefore modify both terms of Eq. (2):

$$\frac{dT_p}{dt} = U\left(T_g - T_p\right)\frac{4\pi R_p^2(1-\varepsilon)}{c_{p,p}m_p} - \frac{h_{fg}\dot{m}_{eff}\alpha}{c_{p,p}m_p} \tag{19}$$

Here, U is given by:

$$\frac{1}{U} = \frac{1}{h} + \frac{R_p - R_i}{k_{cr}} \tag{20}$$

in which R_i is the radius of the interface between the crust and wet core, and k_{cr} is the thermal conductivity of the crust. In the second term of the RHS of (20) it is assumed that the crust is sufficiently thin to be considered as a flat layer. This second term, however, may safely be ignored anyhow, as it is small with respect 1/h given still Bi ≤ 0.1.

Now, we assume that the diameter of the pores is much greater than the vapour molecular mean free path. This permits us to utilize the concept of Stefan flow as the transport mechanism of the water vapour through the crust. At the initial stages of crust growth, the crust can still be considered thin and the tortuosity minor, hence providing little resistance to the mass flow from the droplet. To estimate this initial effective mass transport, we add the factor ε to Eq. (7) – to reflect that the pores occupy only part ε of the particle surface – and replace R_p^2 by R_i^2:

$$\dot{m}_{eff} = h_D(\rho_v - \rho_\infty)4\pi R_i^2 \varepsilon \tag{21}$$

As the liquid continues to evaporate from the particle, the interface radius recedes further and further and the crust keeps thickening. As a result, the evaporation rate starts decreasing. The diffusive transport of the vapour through the tortuous capillaries within the crust must then be described in terms of Stefan diffusion (Cengel, 2002; Sadafi et al., 2014; Van den Akker and Mudde, 2023):

$$\dot{m}_{eff} = \frac{M_w 4\pi R_i^2 P_g \varepsilon^{1+\beta} D_v}{(R_p - R_i)\Re T_p} \ln\left(\frac{1-y_\infty}{1-y_v}\right) \tag{22}$$

where P_g is the pressure of the gas phase, y_∞ and y_v are the species molar fractions of the bulk phase and at the particle surface, respectively. As soon as Eq. (22) gives a lower value for $\dot{m}_{eff}$ than Eq. (21), the code switches to the lower evaporation rate of Eq. (22). While in the literature mostly values for the empirical exponent, β, in the range 1.8 and 2.0 have been suggested (Archie, 1942; Golman and Julklang, 2013), we used the value 1.9 in agreement with Golman and Julklang (2013). We are not in favour of using β as a fitting parameter to construct a better agreement with experimental data as done by Mortier et al. (2012).

The decrease in the interface radius as a result of the water evaporation follows from a mass balance for the water. With the dairy components staying where they precipitated, we have to insert porosity ε into an equation resembling Eq. (14):

$$R_i^{n+1} = \sqrt[3]{\frac{4\pi/3(R_i^n)^3\rho_w\varepsilon - \dot{m}_{eff}\Delta t}{4\pi/3\rho_w\varepsilon}} \tag{23}$$

The total particle mass is then calculated as the sum of the mass of the inner wet core (denoted by the subscript co) and the dry crust (denoted by the subscript cr):

$$m_p = 4\pi/3R_i^3\rho_{co} + 4\pi/3\left(R_p^3 - R_i^3\right)\rho_{cr} \tag{24}$$

where ρ_{co} and ρ_{cr} stand for the respective densities of the wet core and the crust, to be calculated from

$$\rho_{co} = \phi\rho_{SMP} + (1-\phi)\rho_w \tag{25}$$

and

$$\rho_{cr} = (1-\varepsilon)\rho_{SMP} \tag{26}$$

We now modify Eq. (15) to account for the porosity within the crust. This provides us with the following equation to calculate the new averaged density of the particle (ignoring the voids within the crust):

$$\rho_p = \frac{m_p}{4\pi/3\left[\varepsilon(R_i^{n+1})^3 + (1-\varepsilon)R_p^3\right]} \tag{27}$$

From this, the moisture content can be calculated on the analogy of Eq. (16). As soon as the mass flow rate of liquid from the particle becomes greater than the amount remaining in it, the particle is considered to be dry and the final stage of the drying model is entered.

2.5. The equations for the inert heating regime

As the moisture content of the particle reaches the final bounded level, inert heating begins. Since the mass flow rate of liquid from the droplet reaches zero, no evaporative cooling is observed by the particle. The evaporative cooling term of Eq. (19) then vanishes and hence the heat transfer from the gas phase just heats the porous particle, as still Bi ≤ 0.1 :

$$\frac{dT_p}{dt} = U\left(T_g - T_p\right)\frac{4\pi R_p^2(1-\varepsilon)}{c_{p,p}m_p} \tag{28}$$

The combination of the above three drying regimes permits us to analyse and predict the interactions between a particle and the gas phase during drying. This model can be applied by using moderate computational resources provided that composition and physical properties of the material we are looking to dry are known.

2.6. Running simulations

The model was initially implemented and prototyped in Spyder using the programming language Python 2.7. The code was run for initial conditions for the droplet and ambient flow parameters estimated to be equal to those in specific single droplet drying experiments. Functions were iterated over time using a time step of 0.05s and were stopped as soon as the simulation time had reached the recorded time duration of the experiment. During the simulations, the (uniform) particle temperature was tracked along with the particle mass.

In a later stage, the prototyped model was implemented into the CFD software ANSYS/Fluent by means of a user defined function routine through C programming. The numerical domain was a duct for air flowing over a prescribed droplet. The domain was spatially discretized by using structured hexahedral cells and was large enough to ensure walls or boundaries did not have an impact on the air flow around the droplet. Comparisons between the Python model and the CFD model showed negligible differences and hence only the results obtained with ANSYS/Fluent are reported here.

3. Matching simulations and experimental data

3.1. Dairy properties in the simulations

Our novel drying model was validated with the help of experimental literature data (Lin and Chen, 2002; Chen et al., 1999; Nešić, 1989; Nešić and Vodnik, 1991) on drying a single droplet of skim milk powder (SMP). The five experimental cases used in our validation study are listed in Table 1. Such a validation study requires all input parameters needed in the model are reported in these papers. Since this is not the case, several assumptions with respect t the dairy properties had to be made.

Lin and Chen (2002) report the gross composition of their SMP which is reproduced in Table 2. We have used this typical composition for all our simulations since the other papers do not specify a composition.

In Table 3, we report expressions for density, thermal conductivity and specific heat of relevant skim milk constituents as a function of temperature (in °C) taken from Choi and Okos (1986). We assume that the data in Table 3 are representative of the SMPs used in the experiments reported in the above papers (Lin and Chen, 2002; Chen et al., 1999; Nešić, 1989; Nešić and Vodnik, 1991).

By using the gross composition from Table 2 and the component properties from Table 3, composite material properties of a typical SMP can be calculated as presented at the bottom of Table 3. These material properties, however, are not identical to powder properties, since the powder particles used in the experiments are porous. Their porosity ε_0 is needed to convert material density into powder density according to

$$\rho_p = (1-\varepsilon_0)\rho_{SMP} \tag{29}$$

which is equivalent to Eq. (17).

Lin and Chen (2002) report they used SMP purchased from a local market to make up reconstituted milk at a certain weight percentage,

Table 1
Experimental parameters for single droplet drying as reported by the experimentalists: initial droplet diameter, air velocity, initial droplet temperature, and air temperature.

Case A (Lin and Chen, 2002)	Diameter	1.44 mm
	Velocity	0.45 m/s
	Drop temp	23.4 °C
	Air temp	67.5 °C
Case B (Lin and Chen, 2002)	Diameter	1.44 mm
	Velocity	0.45 m/s
	Drop temp	28.5 °C
	Air temp	87.1 °C
Case C (Lin and Chen, 2002)	Diameter	1.41 mm
	Velocity	0.45 m/s
	Drop temp	32.0 °C
	Air temp	106.6 °C
Case D (Chen et al., 1999)	Diameter	2.00 mm
	Velocity	1.3 m/s
	Drop temp	8.5 °C
	Air temp	70 °C
Case E (Nešić, 1989; Nešić and Vodnik, 1991)	Diameter	1.71 mm
	Velocity	0.75 m/s
	Air temp	90 °C

Table 2
SMP gross composition (Lin and Chen, 2002).

Protein	36.5
Lactose	49.8
Fat	0.6
Minerals	9.3
Moisture	3.8

Table 3
Physical properties (density ρ_i, thermal conductivity k_i and specific heat $c_{p,i}$ of the SMP components i present in mass fraction x_i) with T in °C, taken from Choi and Okos (1986), plus the composite physical properties of SMP.

Water	
	$\rho_w = 997.18 + 3.1439\times10^{-3}T - 3.7574\times10^{-3}T^2$
	$k_w = 0.57109 + 1.7625\times10^{-3}T - 6.7036\times10^{-6}T^2$
	$c_{p,w} = 4.1762\times10^{3} - 9.0864\times10^{-2}T + 5.4731\times10^{-3}T^2$
Protein	
	$\rho_{pr} = 1329.9 - 0.5185T$
	$k_{pr} = 0.17881 + 1.1958\times10^{-3}T - 2.7178\times10^{-6}T^2$
	$c_{p,pr} = 2.0082\times10^{3} + 1.2089T - 1.3129\times10^{-3}T^2$
Lactose	
	$\rho_c = 1599.1 - 0.31046T$
	$k_c = 0.20141 + 1.3874\times10^{-3}T - 4.3312\times10^{-6}T^2$
	$c_{p,c} = 1.5488\times10^{3} + 1.9625T - 5.9339\times10^{-3}T^2$
Fat	
	$\rho_f = 925.59 - 0.41757T$
	$k_f = 0.18071 - 2.7604\times10^{-3}T - 1.7749\times10^{-7}T^2$
	$c_{p,f} = 1.9842\times10^{3} + 1.4733T - 4.8008\times10^{-3}T^2$
Minerals	
	$\rho_m = 2423.8 - 0.28063T$
	$k_m = 0.17881 + 1.1958\times10^{-3}T - 2.7178\times10^{-6}T^2$
	$c_{p,m} = 2.0082\times10^{3} + 1.2089T - 1.3129\times10^{-3}T^2$
SMP	
	$1/\rho_{SMP} = x_w/\rho_w + x_{pr}/\rho_{pr} + x_c/\rho_c + x_f/\rho_f + x_m/\rho_m$
	$k_{SMP} = x_w k_w + x_{pr}k_{pr} + x_c k_c + x_f k_f + x_m k_m$
	$c_{p,SMP} = x_w c_{p,w} + x_{pr}c_{p,pr} + x_c c_{p,c} + x_f c_{p,f} + x_m c_{p,m}$

viz. 20%. Since our model is in terms of volume fractions, their mass fraction has to be converted in a volume fractions. Let x_0 (=0.20) be the mass fraction of SMP in their solution (denoted by subscript sol) obtained by dissolving a volumetric quantity V_{powder} of SMP to give a volume V_{sol} of the solution. This x_0 follows from

$$x_0 = \frac{\rho_{SMP}(1-\varepsilon_0)V_{powder}}{\rho_{sol}V_{sol}} \tag{30}$$

By defining

$$\phi_0 = \frac{V_{powder}}{V_{sol}} \tag{31}$$

the density of the dairy solution can be written as:

$$\rho_{sol} = \phi_0(1-\varepsilon_0)\rho_{SMP} + (1-\phi_0)\rho_w \tag{32}$$

Substituting Eq. (32) into Eq. (30) and rearranging gives an equation for ϕ_0 :

$$\phi_0^{-1} = 1 + \frac{(1-\varepsilon_0)(1-x_0)}{x_0}\frac{\rho_{SMP}}{\rho_w} \tag{33}$$

showing that we need a value for porosity ε_0. Unfortunately, neither the value of ε_0 nor a value for ϕ_0 was reported in the above papers (Lin and Chen, 2002; Chen et al., 1999; Nešić, 1989; Nešić and Vodnik, 1991).

An estimated value of ϕ_0 can be obtained, however, by dividing the reported particle mass at the end of the drying experiment by the reported initial mass of the droplet. For the experiments used in this validation study, this ratio is in the range 0.25–0.285. Given Eq. (33), the corresponding values of ε_0 are then in the range 0.5–0.6.

Given the uncertainty in these estimated ϕ_0 and ε_0 values, simulations were carried out for just two fixed values of these input parameters: $\varepsilon_0 = 0.55$ (with $\phi_0 = 0.27$) and $\varepsilon_0 = 0.60$ (with $\phi_0 = 0.294$).

While in general powder porosity may depend on the drying conditions, such as the rate of drying and the temperature of the drying air, it is assumed – for lack of further information or evidence – that porosity is independent of such conditions. This implies that in our simulations the porosity ε of the crust was assumed to be equal to ε_0 of the original SMP.

The thermal conductivity and the specific heat of the solution are calculated by means of:

$$k_{sol} = \phi_0 k_{SMP} + (1-\phi_0)k_w \tag{34}$$

$$c_{p,sol} = \phi_0 c_{p,SMP} + (1-\phi_0)c_{p,w} \tag{35}$$

Throughout the simulation, Eqs. (32), (34) and (35) though with ϕ rather than with ϕ_0 are updated in every time step by using Eq. (16) in order to keep track of the increasing solid content due to the liquid evaporation.

3.2. Experimental issues

Before we turn to the results of our validation study, we have to communicate some observations about the drying experiments reported by Lin and Chen (2002). These observations were triggered by our finding that we had to assume a lower air temperature than reported by Lin and Chen to get a good overall agreement between our simulation results and the experimental data on both particle temperature and mass as a function of time.

In addition, the particle temperatures in the Lin and Chen experiments all exhibit a drop at the start of the experiments and then stay lower for some 30 to 40 s. This initial temperature decay is indicative of a lower air temperature such that much of the heat for the evaporation was taken from the droplet (see also the first paragraph of Section 2.1). In our simulations, the droplet temperature remains constant or increases, indicating the heat for the evaporation is provided by the air.

Lin and Chen describe extensively how they operated their test rig which contained a bypass used to keep the hot air running while positioning the glass filament and the droplet attached to it in the actual drying compartment. They had to wait until the droplet had reached a stable position, before restoring the hot air flow to the drying compartment to start the experiment.

Our interpretation of their temperature data is that, due to the interruption of the air flow and the instalment of filament and droplet, the (air in the) drying compartment was no longer at the targeted temperature at the start of the drying process. In all cases, it took some 50 s

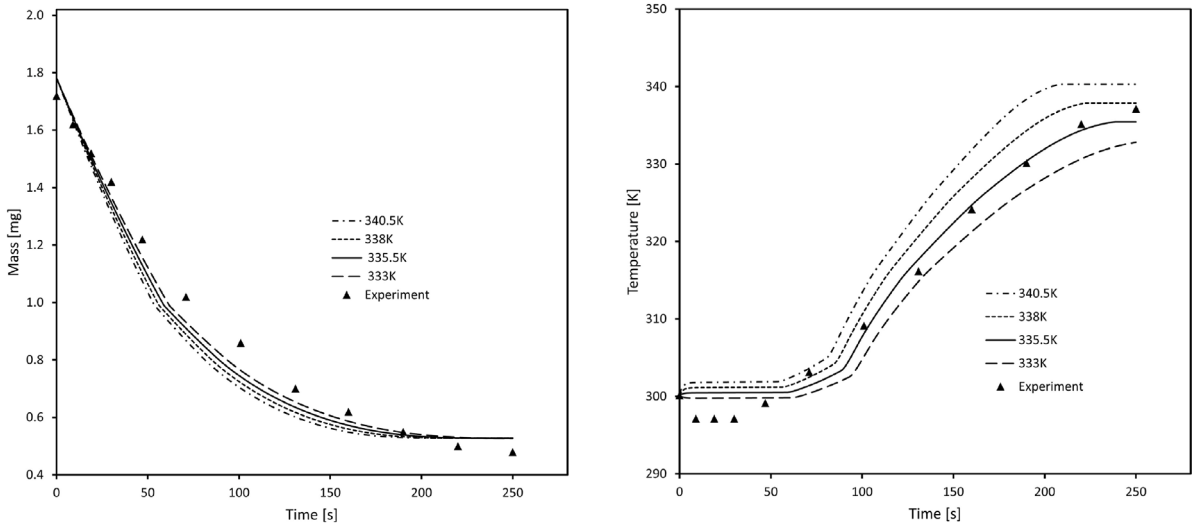

Fig. 2. Particle mass (left panel) and particle temperature (right panel) for Case A both as a function of time; the model was run for four different constant air temperatures (340.5 K, 338 K, 335.5 K, 333 K) and with $\varepsilon_0 = 0.55$, $\phi_0 = 0.27$ (see Eq. (31) for definition of ϕ_0).

before the droplet was at its initial temperature again. Note the entire drying process took sone 200 s only. Still in our interpretation, only after the initial 50 s, air temperature in the drying compartment was high enough to provide the heat for the evaporation. This temperature recovery could easily take another 50 s or more. Since we do not have the option of a variable air temperature in our code, we carried out simulations for several lower average air temperatures to explore and demonstrate the above observations.

The experiments reported by Chen et al. (1999) were carried out in an earlier version of the test rig, given the description in Stevenson et al. (1998). The same remarks as above with respect to the data reported by Lin and Chen (2002) may apply here as well.

4. Validation of the drying model

As Lin and Chen (2002) report more details and conditions of their experiments than the other authors, and their experimental procedure look most sophisticated (in spite of the above observations), we first simulated a few of their experiments (Cases A, B and C of Table 1) with the view to validating our model. Afterwards, we used data reported by Chen et al. (1999) and by Nešić (Nešić, 1989; Nešić and Vodnik, 1991) in the validation Cases D and E, respectively.

4.1. Case A

Fig. 2 shows for Case A, with $\varepsilon_0 = 0.55$, $\phi_0 = 0.27$, how during the drying process, according to our model and in the experiment, particle mass decreases with time and particle temperature mostly increases with time. In our model, four different constant air temperatures were applied, to explore and demonstrate the effect of different air temperatures as discussed in section 3.2. All four temperature profiles in Fig. 2 exhibit kinks which signal transitions in drying regime: after some 55 s, the constant drying rate regime is over, while Stefan diffusion becomes the rate determining step after about 90 s, and after 200 s the inert heating regime is entered. Only the first transition is clearly visible in the plots of particle mass versus time as at that moment in time the crust starts affecting the evaporation rate.

Fig. 2 shows that the lower particle temperature during the first, say, 30 s of the experiment is not reproduced by the simulations. In addition, using the air temperature of 340.5 K (67.5 °C) reported in Lin and Chen (2002) as input to the simulation results in a distinct over-prediction of particle temperatures in the falling rate regime. Both findings gave rise to the conclusion in section 3.2 that at the start of the Lin and Chen experiments air temperature in the drying chamber suffered from a temporary dip long and big enough to seriously affect most of the drying process.

Therefore, air temperature was decreased in the computer runs in steps of 2.5 K to find out about the probable drop in air temperature in the experiment. A constant (or averaged) air temperature of 335.5 K (62.5 °C) looks as the best estimate. The effect of air temperature on particle mass as a function of time looks rather limited: a lower air temperature results in just a slightly slower decrease in particle mass.

Fig. 3 presents very similar effects for simulations with $\varepsilon_0 = 0.60$, $\phi_0 = 0.294$. It is difficult to judge the difference between the cases $\varepsilon_0 = 0.55$, $\phi_0 = 0.27$ (in Fig. 2) and $\varepsilon_0 = 0.60$, $\phi_0 = 0.294$ (in Fig. 3) when plotted separately. Therefore, two typical cases for the 'optimal' average air temperature of 335.5 K (62.5 °C) have been plotted in Fig. 4: the cases $\varepsilon_0 = 0.55$, $\phi_0 = 0.27$ and $\varepsilon_0 = 0.60$, $\phi_0 = 0.294$. The effect on the temperature history is limited, but the higher values for ε_0 and ϕ_0 do result in a lower value for the final particle mass, in line with the discussion in section 3.2 on estimating a value for ε_0 in the experiment.

4.2. Case B

We repeated a similar validation exercise for Case B. Fig. 5 presents particle mass (left) and particle temperature (right) as a function of time, again according to our model and in the experiment. The model was run for three different air temperatures and with $\varepsilon_0 = 0.55$, $\phi_0 = 0.27$. Similarly, Fig. 6 does the same for $\varepsilon_0 = 0.60$, $\phi_0 = 0.294$.

From a comparison between Figs. 5 and 6 it is obvious that $\varepsilon_0 = 0.60$, $\phi_0 = 0.294$ is the better choice, given the better reproduction of the final particle mass, although then the gradient in the particle mass is reproduced less well. Figs. 5 and 6 once more demonstrate that using the air temperature (360.25 K or 87.1 °C) reported in Lin and Chen (2002) leads in the model to a substantial over-prediction of particle temperature in the falling rate regime. A lower air temperature (353K or 350 K) results in a better agreement between model prediction and experimental data, irrespective of the values of ε_0 and ϕ_0. After 150 s, particle temperature becomes constant in the model as it reaches the constant air temperature level. In the experiment, particle temperature keeps rising as by then the air temperature recovering from its initial dip was returning to its targetted value. In hindsight, this effect is weakly visible in Case A as well.

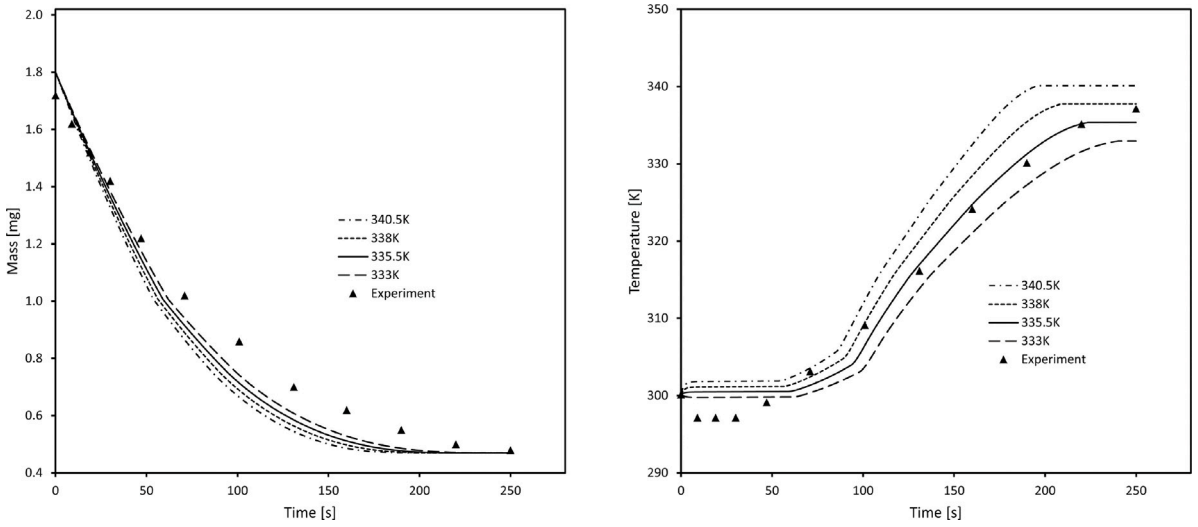

Fig. 3. Particle mass (left panel) and particle temperature (right panel) for Case A both as a function of time; the model was run for four different constant air temperatures (340.5 K, 338 K, 335.5 K, 333 K) and with $\varepsilon_0 = 0.60$, $\phi_0 = 0.294$.

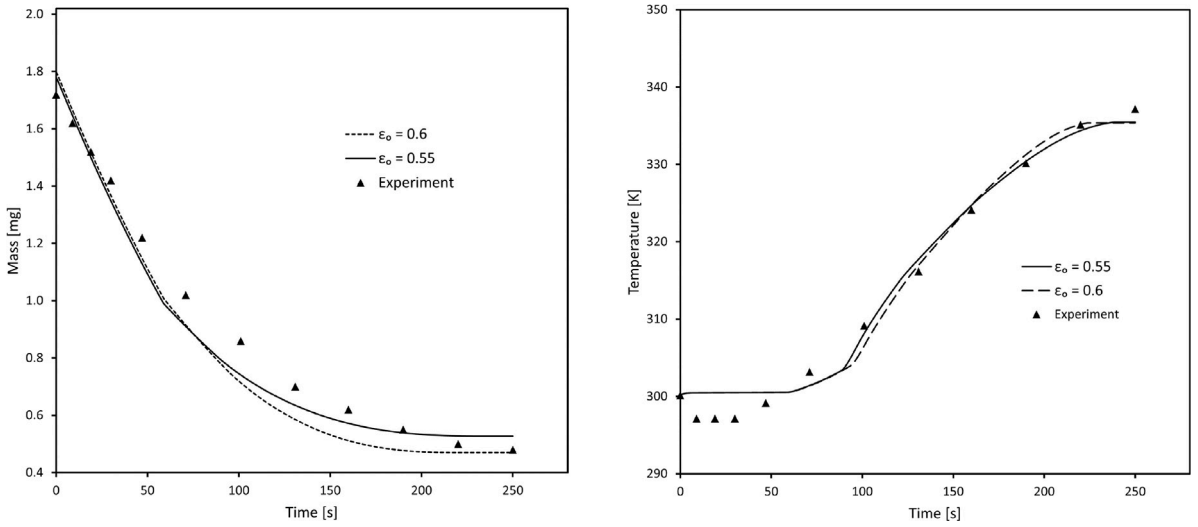

Fig. 4. Particle mass (left panel) and particle temperature (right panel) for Case A both as a function of time, for a constant air temperature of 335.5 K, with $\varepsilon_0 = 0.55$ and 0.60.

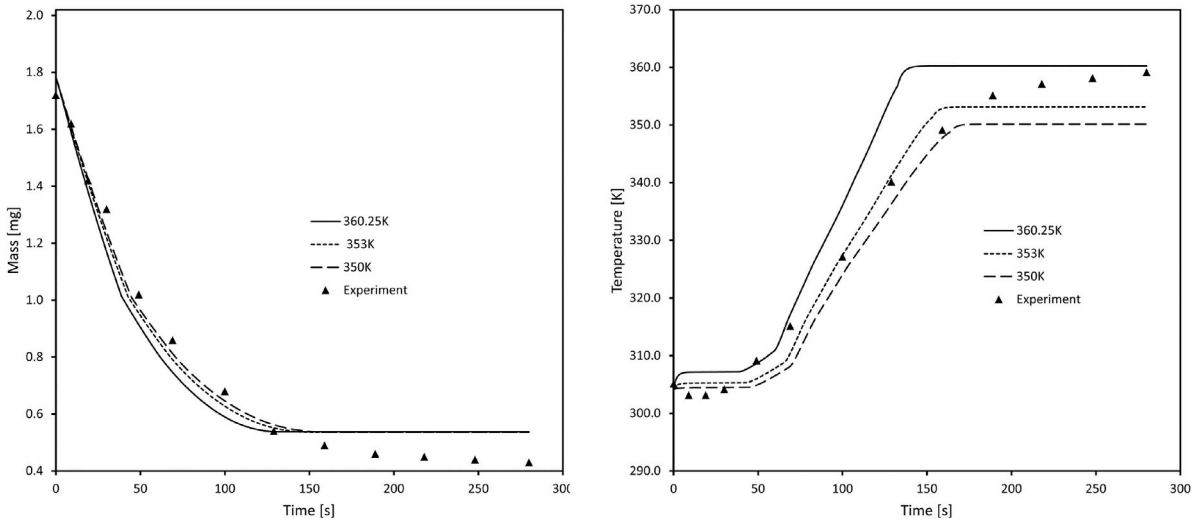

Fig. 5. Particle mass (left panel) and particle mass (right panel) for Case B as a function of time; the model was run for three different constant air temperatures (360.25 K, 353 K, 350 K) with $\varepsilon_0 = 0.55$, $\phi_0 = 0.27$.

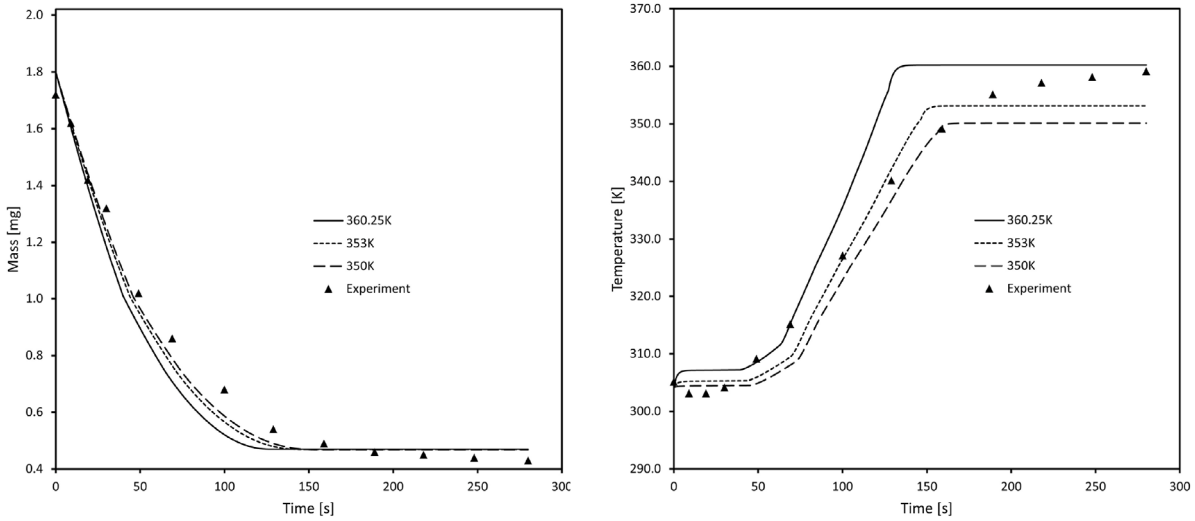

Fig. 6. Particle mass (left panel) and particle mass (right panel) for Case B as a function of time; the model was run for three different constant air temperatures (360.25 K, 353 K, 350 K) with $\varepsilon_0 = 0.60$, $\phi_0 = 0.294$.

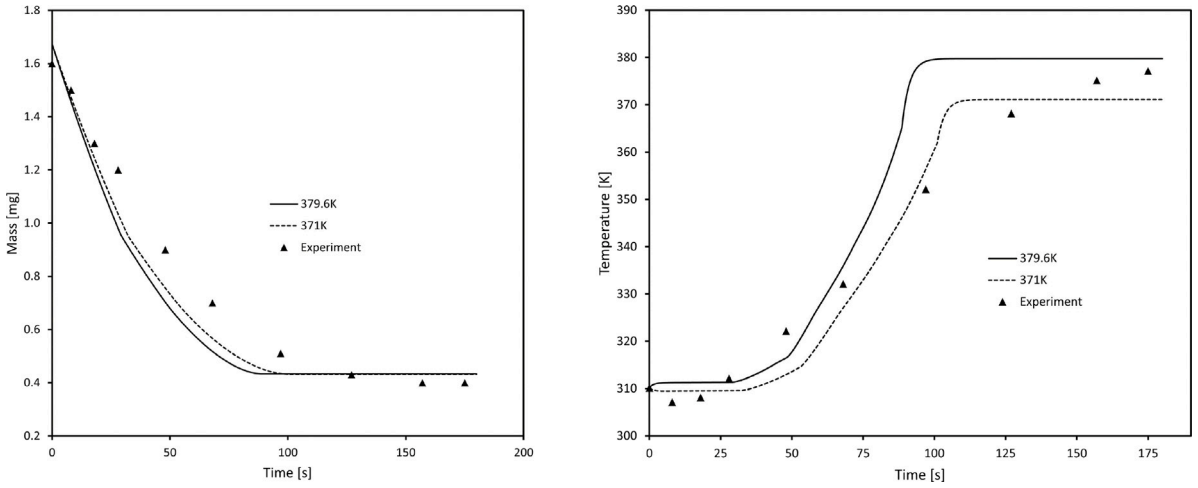

Fig. 7. Particle mass (left panel) and particle temperature (right panel) for Case C as a function of time; the model was run for two different constant air temperatures (379.6 K, 371 K) with $\varepsilon_0 = 0.60$.

4.3. Case C

A similar validation exercise was done for Case C the results of which are shown in Fig. 7. Given the findings in Cases A and B, only the higher values for ε_0 and ϕ_0 are shown. Applying the targeted air temperature (379.6 K, or 106.6 °C) in the simulation really over-predicts particle temperatures in the falling rate regime. After, say, 80 s, a clear kink and a steep increase are found with air and particle temperatures close to the boiling point of water.

Substituting a lower air temperature brings the simulation results for both particle mass and particle temperature closer to the experimental data. Since the effect of the initial drop in air temperature on the drying process was expected to increase with higher air temperatures, particularly close to and in excess of the boiling point of water, a more extended analysis of this case was not considered very useful.

4.4. Summary of Cases A, B and C

In all three Cases A through C, we found that a (constant) lower air temperature results in a better overall reproduction of the experimental drying process of a single SMP droplet. This applies to particle temperature rise and to a lesser degree also to particle mass. In addition, in all cases, particle temperatures dropped at the start of the drying experiments, while in the simulations droplet temperatures remained constant or increased, depending on the air temperature. The above findings, consistent throughout all three Cases, were at the basis of the discussion in Section 3.2 on the drying experiments reported by Lin and Chen (2002). The temporary drop in air temperature in the experiments was found to be larger for higher air temperatures. Of course, by assuming a lower constant air temperature the final experimental particle temperature was not reproduced correctly. The latter would require a varying air temperature; this was beyond the scope of the current paper.

The initial porosity ε_0 of the SMP particles was not explicitly reported in Lin and Chen (2002) and could only be estimated afterwards from the initial and final particle mass in the drying experiment, thanks to Eq. (33). Since the initial porosity in the three cases was in the range 0.5–0.6, the effect of using both 0.55 and 0.6 for ε_0 (and the corresponding values for ϕ_0) was investigated. The (tentative) conclusion was that ε_0=0.6 gives a better agreement with the experimental data, particularly with respect to the final particle mass.

We did not investigate the effect of air velocity and air humidity. We explored the impact of several modifications in the model but they all did not result in a better agreement with the experimental data.

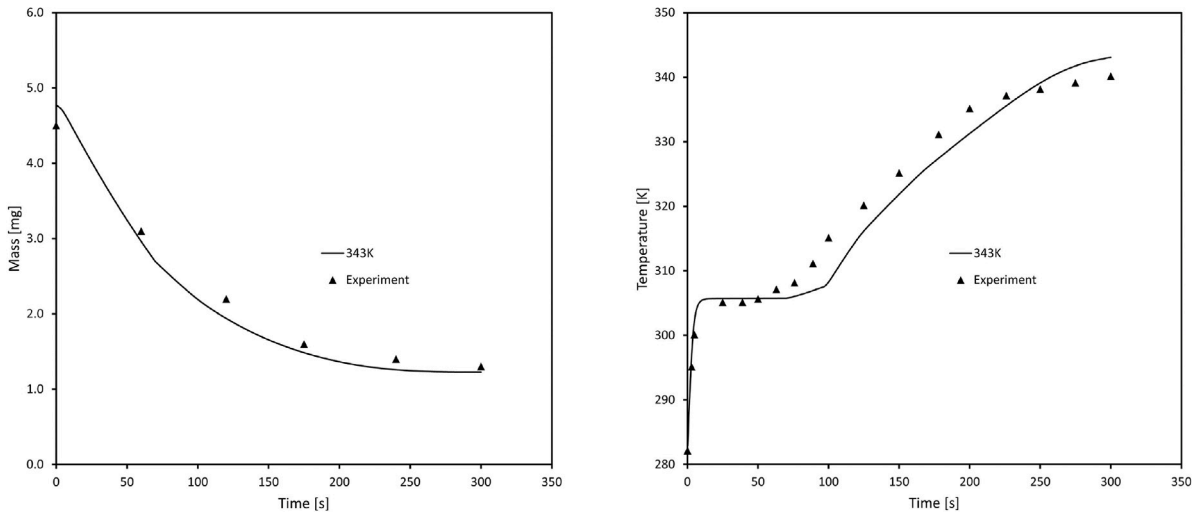

Fig. 8. Particle mass (left panel) and particle temperature (right panel) for Case D as a function of time, for air temperature 343 K and with ε_0 = 0.60.

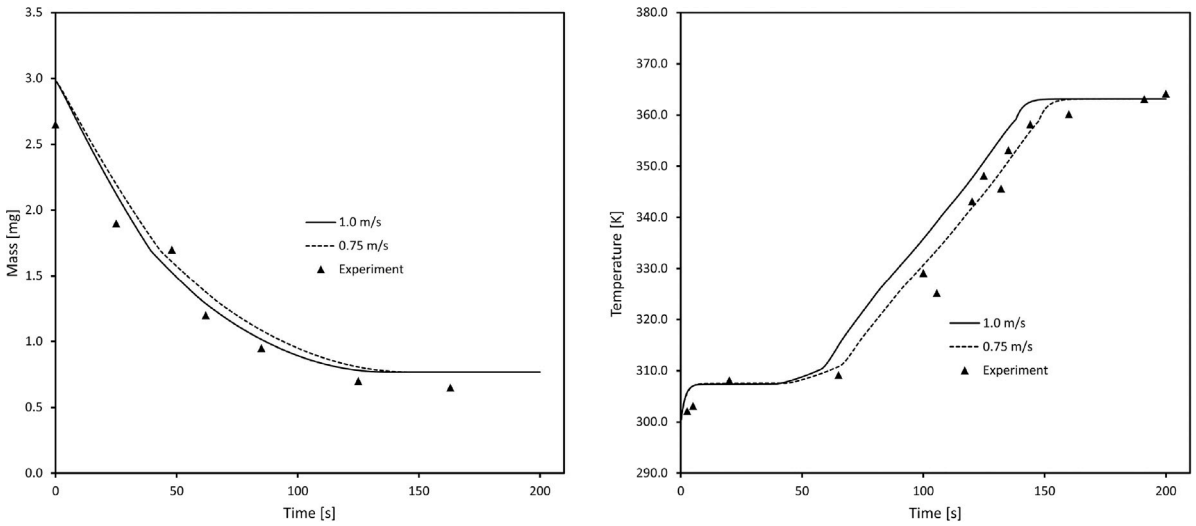

Fig. 9. Particle mass (left panel) and particle temperature (right panel) for Case E as a function of time, for air temperature 363 K and with ε_0 = 0.60; the model was run for two air velocities: 0.75 m/s and 1.0 m/s.

Varying the parameter β in Eq. (22) had a minor effect only. Using Eq. (10), from Lin and Chen (2002), for the Nu number rather than Eq. (8) did not make a noticeable difference.

We did not decouple crust porosity from the estimated porosity of Lin and Chen's SMP; due to the lack of knowledge about the effect of drying conditions and physical properties on deposition and resulting porosity, such decoupling would come to artificially matching the model to experimental data without proper physical background. Lowering the air temperature was the only option to get a good agreement with the experimental particle temperature and mass data.

4.5. Case D

Given the above findings, we decided to assess our drying model also with older experimental data. First, in Case D, we looked at drying experiments reported by Chen et al. (1999). Their experiments were carried out in an earlier version of the test rig at the University of Auckland as described by Stevenson et al. (1998). The drying conditions of Case D differ from those of Cases A through C due to a substantially higher air velocity and a somewhat larger droplet size. The resulting higher drying rates may make the simulations less sensitive to other parameters.

Fig. 8 presents a comparison between our simulations with a ε_0 value of 0.60 and the experimental data from Chen et al. (1999). We assumed the same type of SMP was used as by Lin and Chen. A very satisfactory agreement is found with almost perfectly fitting slopes of particle mass and temperature versus time. In this experiment, an initial drop in particle temperature was not observed, and also using the reported value for the air temperature did not result in too high particle temperatures in the simulation.

4.6. Case E

A final check was done with the help of the experimental drying data reported by Nešić. The Nešić data suffer from a high degree of uncertainty: while Nešić (1989) only reported the temperature of the drying air, Nešić and Vodnik (1991) also reported droplet size, air velocity and milk fat percentage for the same Nešić 1989 experiment. Further details about the SMP were not reported. For the simulation of the same Nešić experiment, Farid (2003) applied a different air velocity (1.0 m/s, rather than the 0.75 m/s reported in Nešić and Vodnik (1991)) and started from a slightly different droplet size, while again assuming 20wt% skim milk.

As shown in Fig. 9, the agreement between experimental data and simulation results is very satisfactory. This might be coincidental as Nešić did neither specify the composition of his SMP nor the porosity and we just used the composition data reported by Lin and Chen. We also investigated the effect of applying a higher air velocity to double check the potential merit of using Farid's higher value (Farid, 2003): however, Nešić's lower value gave a better agreement with the experimental particle temperature data.

4.7. Overall summary of the validation study

The results of the successful validation study demonstrate the ability of the novel numerical model to computationally simulate the drying process of a single SMP droplet. Although the experimental data were taken from three sources and, due to lack of reported data, some assumptions had to be made, the agreement between the simulated and experimental particle mass and temperature histories was very satisfactory. On the basis of a sensitivity study on the impact of various modelling aspects, the code has turned out be very robust. With respect to the experimental data reported by Lin and Chen (2002), we found that their drying experiments in what looks as a very sophisticated test setup, suffered from a problem associated with interrupting the hot air flow to allow for the instalment of the droplet into their drying chamber.

The benefit of this novel model is that there are no tuning or experimental calibration required as input. The only information required for simulating the drying process of a (single) dairy droplet is about the material properties of the various constituents making up a dairy product which can be found in Choi and Okos (1986). This way, the effects of dairy composition, of the initial particle diameter, porosity and temperature, and of a constant air temperature and velocity can be assessed computationally.

5. Conclusions

This paper details the development of a novel numerical modelling approach for drying a dairy droplet. The drying model distinguishes between three regimes, viz. unhindered evaporation, restricted drying, and finally inert heating. The unhindered evaporation and the inert heating regimes are described in terms of common basic heat transfer principles. The restricted, or falling rate, drying regime is due to a crust growing around a wet core and imposing a limitation to the transport of water vapour towards the particle surface. This is accounted for by Stefan diffusion through the capillary pores in the crust. The temperature inside the droplet/particle is assumed to be uniform since the value of the Biot number greatly exceeds unity. The combination of these aspects is unprecedented. Material properties are calculated as a function of composition and temperature; this eliminates the need of experimental testing of each product subjected to droplet drying.

The novel model is validated against experimental work carried out on single droplet drying as reported in the literature. A good agreement is observed between the numerical results and experimental data from three sources. Our findings strongly suggest that the Lin and Chen (2002) experiments suffered in their early phase from a dip in the air temperature. This temporary temperature drop was accounted for by lowering in Cases A, B and C the constant air temperature applied to the model, with the view of getting a good agreement with the Lin and Chen data. In Cases D (Chen et al., 1999) and E (Nešić, 1989), the agreement between our model and the experimental data was very good without such an adjustment.

Our numerical model does not require input from experiments or empirical correlations as required in the so-called reaction engineering approach. This indicates the model presented here can really forecast the drying process of a dairy droplet, provided just the composition and the physical properties of the dairy product are known. The result is a computationally efficient, robust and reliable numerical model with a good accuracy, ready for application to more elaborate droplet drying studies. With the new model, the effects of dairy composition, of the initial particle diameter, porosity and temperature, and of a constant air temperature and velocity can be assessed computationally, i.e. without delicate and expensive experimental testing.

Future work could involve incorporating the developed model into a (commercial) CFD solver for the flow field of the hot air in a spray drier. This will further enhance the knowledge of the complex and intimately coupled transport processes within a given spray drying chamber and will allow for the optimization or de-bottlenecking of the overall spray drying process.

Declaration of competing interest

The authors declare that they have no known competing financial interests or personal relationships that could have appeared to influence the work reported in this paper.

Acknowledgements

The authors would like to acknowledge the Dairy Processing Technology Centre (DPTC), an Enterprise Ireland initiative, for financial support and permission to publish this work. This work was supported by the Irish State through funding from the Technology Centres Programme (Grant Number TC/2014/0016).

References

Archie, G.E., 1942. The electrical resistivity log as an aid in determining some reservoir characteristics. Trans. AIME 146 (01), 54–62.
Cal, Krzysztof, Sollohub, Krzysztof, 2010. Spray drying technique. I: Hardware and process parameters. J. Pharm. Sci. 99 (2), 575–586.
Cengel, Yunus A., 2002. Heat Transfer: A Practical Approach, second ed. McGraw-Hill, p. 896.
Charlesworth, D.H., Marshall, Jr., W.R., 1960. Evaporation from drops containing dissolved solids. AIChE J. 6, 6–23.
Chen, X.D., 2008. The basics of a reaction engineering approach to modeling air drying of small droplets or thin layer materials. Dry. Technol. 26, 627–639.
Chen, X.D., Farid, M.M., Reid, D., Fletcher, A., Pearce, D., Chen, N.X., 1999. A new model for the drying of milk droplets for fast computation purposes. In: CHEMECA99 - Chemical Engineering: Solutions in a Changing Environment, Newcastle, Australia. The Institution of Engineers, Australia, pp. 865–870.
Chen, Xiao Dong, Putranto, Aditya, 2015. Reaction engineering approach (REA) to modeling drying problems: recent development and implementations. Dry. Technol. 33, 1899–1910.
Choi, Y., Okos, M.R., 1986. Effects of temperature and composition on the thermal properties of foods. In: Food Engineering and Process Applications, Vol.1 - Transport Phenomena. Elsevier Applied Science Publishers, pp. 93–101.
Deen, William M., 1998. Analysis of Transport Phenomena. Oxford University Press.
Farid, Mohammed, 2003. A new approach to modelling of single droplet drying. Chem. Eng. Sci. 58, 2985–2993.
Gabites, J.R., Abrahamson, J., Winchester, J.A., 2010. Air flow patterns in an industrial milk powder spray dryer. Chem. Eng. Res. Des. 88 (7), 899–910.
Golman, Boris, Julklang, Wittaya, 2013. Analysis of drying kinetics of a slurry droplet in the falling rate period of spray drying. Int. J. Chem. Mol. Eng. 7 (9), 685–689.
Gopireddy, S.R., Gutheil, E., 2013. Numerical simulation of evaporation and drying of a bi-component droplet. Int. J. Heat Mass Transfer 66, 404–411.
Haque, M. Amdadul, Adhikari, Benu, Putranto, Aditya, 2016. Predictions of drying kinetics of aqueous droplets containing WPI-lactose and WPI-trehalose by application of composite reaction engineering approach (REA). J. Food Eng. 189, 29–36.
Harvie, D.J.E., Langrish, T.A.G., Fletcher, D.F., 2001. Numerical simulations of gas flow patterns within a tall-form spray dryer. Chem. Eng. Res. Des. 79 (3), 235–248.
Jaskulski, M., Wawrzyniak, P., Zbicinński, I., 2018. CFD simulations of droplet and particle agglomeration in an industrial counter-current spray dryer. Adv. Powder Technol. 29, 1724–1733.
Jin, Yan, Chen, Xiao Dong, 2009. Numerical study of the drying process of different sized particles in an industrial-scale spray dryer. Dry. Technol. 27 (3), 371–381.
Jubaer, Hasan, Afshar, Sepideh, Xiao, Jie, Chen, Xiao Dong, Selomulya, Cordelia, Woo, Meng Wai, 2018. On the importance of droplet shrinkage in CFD-modeling of spray drying. Dry. Technol. 36, 1785–1801.
Kašpar, O., Tokárová, V., Oka, S., Ramachandran, R., Štěpánek, F., 2013. Combined UV/VIS amnd micro-tomography investigation of acetaminophen dissolution from granules. Int. J. Pharm. 458, 272–281.
Kieviet, F.G., Kerkhof, P.J.A.M., 1997. Air flow, temperature, and humidity patterns in a co-current spray dryer: modelling and measurements. Dry. Technol. 15, 1763–1773.

Langrish, T.A.G., Kockel, T.K., 2001. The assessment of a characteristic drying curve for milk powder for use in computational fluid dynamics modelling. Chem. Eng. J. 84 (1), 69–74.
Lin, S.X.Q., Chen, X.D., 2002. Improving the glass-filament method for accurate measurement of drying kinetics of liquid droplets. Chem. Eng. Res. Des. 80 (4), 401–410.
Mezhericher, M., Levy, A., Borde, I., 2007. Theoretical drying model of single droplets containing insoluble or dissolved solids. Dry. Technol. 25 (6), 1025–1032.
Mezhericher, M., Levy, A., Borde, I., 2008. Modelling of particle breakage during drying. Chem. Eng. Process.: Process Intensification 47 (8), 1410–1417.
Mezhericher, M., Levy, A., Borde, I., 2010a. Theoretical models of single droplet drying kinetics: A review. Dry. Technol. 28 (2), 278–293.
Mezhericher, M., Levy, A., Borde, I., 2010b. Three-dimensional modelling of pneumatic drying process. Powder Technol. 203 (2), 371–383.
Mezhericher, M., Levy, A., Borde, I., 2011. Modelling the morphological evolution of nanosuspension droplet in constant-rate drying stage. Chem. Eng. Sci. 66 (5), 884–896.
Mezhericher, M., Levy, A., Borde, I., 2012. Probabilistic hard-sphere model of binary particle-particle interactions in multiphase flow of spray dryers. Int. J. Multiph. Flow 43, 22–38.
Mezhericher, Maksim, Levy, Avi, Borde, Irene, 2015. Multi-scale multiphase modeling of transport phenomena in spray-drying processes. Dry. Technol. 33 (1), 2–23.
Moroney, K.M., Vynnycky, M., 2021. Mathematical modelling of drug release from a porous granule. Appl. Math. Model. 432–452.
Mortier, Séverine, De Beer, Thomas, Gernaey, Krist V., Vercruysse, Jurgen, Fonteyne, Margot, Remon, Jean Paul, Vervaet, Chris, Nopens, Ingmar, 2012. Mechanistic modelling of the drying behaviour of single pharmaceutical granules. Eur. J. Pharm. Biopharm. 80 (3), 682–689.
Nešić, S., 1989. The evaporation of single droplets - experiments and modelling. In: Drying '89, Edited by A.S. Mujumbar. Hemisphere Pub. Corp., pp. 386–393.
Nešić, S., Vodnik, J., 1991. Kinetics of droplet evaporation. Chem. Eng. Sci. 46, 527–537.
Putranto, A., Chen, X.D., 2015. An assessment on modeling drying processes: Equilibrium multiphase model and the spatial reaction engineering approach (S-REA). Chem. Eng. Res. Des. 94, 660–672.
Ranz, W.E., Marshall, W.R., 1952. Evaporation from drops. Chem. Eng. Progr. 48, 141–146.
Rezaei, Majid, Netz, Roland R., 2021. Water evaporation from solute-containing aerosol droplets: Effects of internal concentration and diffusivity profiles and onset of crust formatio. Phys. Fluids 33, 091901.
Sadafi, M.H., Jahn, I., Stilgoe, A.B., Hooman, K., 2014. Theoretical and experimental studies on a solid containing water droplet. Int. J. Heat Mass Transfer 78, 25–33.
Sadafi, M.H., Jahn, I., Stilgoe, A.B., Hooman, K., 2015. A theoretical model with experimental verification for heat and mass transfer of saline water droplets. Int. J. Heat Mass Transfer 81, 1–9.
Saleh, Saad Nahi, 2010. CFD simulations of a co-current spray dryer. Int. J. Chem. Mol. Eng. 4 (2), 226–231.
Saleh, Saad Nahi, Hameed, Laith Amjad, 2016. CFD simulation of air flow patterns in a spray dryer fitted with a rotary disk. Iraqi J. Chem. Pet. Eng. 17 (2), 69–77.
Sano, Yuji, Keey, R.B., 1982. The drying of a spherical particle containing colloidal material into a hollow sphere. Chem. Eng. Sci. 37, 881–889.
Sazhin, Sergei S., 2017. Modelling of fuel droplet heating and evaporation: Recent results and unsolved problems. Fuel 196, 69–101.
Sharma, Anup, Jana, Atanu H., Chavan, Rupesh Shrikant, 2012. Functionality of milk powders and milk-based powders for end use applications - A review. Compr. Rev. Food Sci. Food Saf. 11 (5), 518–528.
Shishir, Mohammad Rezaul Islam, Chen, Wei, 2017. Trends of spray drying: A critical review on drying of fruit and vegetable juices. Trends Food Sci. Technol. 65, 49–67.
Sollohub, Krzysztof, Cal, Krzysztof, 2010. Spray drying technique: II. Current applications in pharmaceutical technology. J. Pharm. Sci. 99 (2), 587–597.
Stevenson, Matthew J., Chen, Xiao Dong, Fletcher, Andrew, 1998. The effect of fat content on the drying of milk products. In: Drying '98 - Proc. 11th International Drying Symposium IDS '98, Halkidiki, Greece. Vol. B. pp. 1200–1206.
Strizhak, P.A., Volkov, R.S., Castanet, G., Lemoine, F., Rybdylova, O., Sazhin, S.S., 2018. Heating and evaporation of suspended water droplets: Experimental studies and modelling. Int. J. Heat Mass Transfer 127, 92–106.
Trommelen, A.M., Crosby, E.J., 1970. Evaporation and drying of drops in superheated vapors. AIChE J. 16, 857–867.
Van den Akker, Harry E.A., Mudde, Robert F., 2023. Mass, Momentum and Energy Transport Phenomena: A Consistent Balances Approach, second ed. DeGruyter, Berlin.
Woo, M.W., Che, L.M., Daud, W.RW, Mujumdar, A.S., Chen, X.D., 2012. Highly swirling transient flows in spray dryers and consequent effect on modeling of particle deposition. Chem. Eng. Res. Des. 90 (3), 336–345.
Zhifu, Zhou, Wang, Guoxiang, Chen, Bin, Guo, Liejin, Wan, Yueshe, 2013. Evaluation of evaporation models for single moving droplet with a high evaporation rate. Powder Technol. 240, 95–102.